



A NON-LINEAR LEAST SQUARES SOLUTION  
TO THE PARAMETRIC TRAVEL TIME EQUATIONS

A THESIS SUBMITTED TO THE GRADUATE DIVISION OF THE  
UNIVERSITY OF HAWAII IN PARTIAL FULFILLMENT  
OF THE REQUIREMENTS FOR THE DEGREE OF  
MASTER OF SCIENCE

IN GEOLOGY AND GEOPHYSICS

DECEMBER 1975

TO Kimo -  
with thanks for all  
your "help".  
Bruce

By

Bruce S. Gibson

Thesis Committee:

George H. Sutton, Chairman  
Donald M. Hussong  
Ralph Moberly  
Murli H. Manghnani  
Edwin H. Mookini

We certify that we have read this thesis and that in our opinion it is satisfactory in scope and quality as a thesis for the degree of Master of Science in Geology and Geophysics.

THESIS COMMITTEE

*George H. Fisher*

Chairman

*Clifford H. H.*

*Nahn Moberly*

*Murli H. Manghani*

*Edwin H. Mookini*

## ACKNOWLEDGEMENTS

The author wishes to thank Dr. M. E. Odegard for originally posing the inversion problem and for his continued interest during the work.

## ABSTRACT

The parametric travel time equations are developed for layered media with linear velocity gradients in each layer. The parametric equations provide a straight forward means of reducing multi-layer data to the appropriate single layer case. The velocity-depth relation can then be estimated by using least squares to fit a non-linear model to the reduced data. The regression procedure provides information necessary to construct confidence regions about the estimates.

The inherent inaccuracies of the method are investigated with model studies. Owing to an unsuccessful search for appropriate real data, a theoretical discussion is undertaken on the potential application of this procedure to the study of marine sediments.

## Table of Contents

	Page
ACKNOWLEDGEMENTS . . . . .	iii
ABSTRACT . . . . .	iv
LIST OF TABLES . . . . .	vii
LIST OF FIGURES . . . . .	viii
I. INTRODUCTION . . . . .	1
Previous Approaches . . . . .	2
Other Investigations with the Parametric Equations . . . . .	4
II. THE PARAMETRIC EQUATIONS . . . . .	5
The General Integrals . . . . .	5
Reflections . . . . .	11
Refractions . . . . .	13
Extension to the Multi-Layer Case . . . . .	14
Slope of the Travel Time Curve . . . . .	18
III. SOLUTION OF THE PARAMETRIC EQUATION . . . . .	19
Method . . . . .	19
1. Removal of Effects from Overlying Layers . . . . .	19
2. The Sum of Squares Function . . . . .	21
Reflections . . . . .	22
Refractions . . . . .	23
3. Minimization of the Sum of Squares . . . . .	24
4. Confidence Regions . . . . .	25

	Page
Acceptance Regions . . . . .	31
Results . . . . .	40
IV. DISCUSSION AND CONCLUSIONS . . . . .	49
Physical Problems . . . . .	52
General Problems . . . . .	57
Experimental Problems . . . . .	58
Conclusions . . . . .	64
APPENDIX A: PARAMETRIC TRAVEL TIME EQUATIONS ELLIPTICALLY ANISOTROPIC CASE . . . . .	66
APPENDIX B: INTERVAL VELOCITIES--PARAMETRIC APPROACH . . . . .	68
REFERENCES . . . . .	69

List of Tables

Table		Page
1	The five parameter sets used to test the regression procedure. In every model, layer 1 is a water column ( $v = 1.5$ km/sec, $h = 4.0$ km). Velocity gradients in $\text{sec}^{-1}$ , velocities in km/sec and thicknesses in km . . . . .	35
2	Estimates of the velocity gradient in layers of model taken from Maynard (1973) (ASPER D-12) . . . . .	61

## List of Figures

Figure		Page
1	General ray path in a half-space with a linear increase of velocity with depth . . . . .	6
2	Reflection (PQR) and refraction (PQ'R') ray paths in a layer with a linear velocity gradient . . . . .	6
3a	Reflection ray path and travel time curve--multi-layer case . . . . .	16
3b	Total internal refraction ray path and travel time curve--multi-layer case . . . . .	16
4	Confidence regions about an estimate $\hat{\gamma}, \hat{b}$ for $\alpha = 75, 90$ and $99\%$ . . . . .	28
5	Flow chart of the computer program used to evaluate acceptance limits . . . . .	33
6	Velocity-depth profile of typical test model ( $T_o = .12$ sec) . . . . .	37
7	Comparison of reflection travel time curves and velocity-depth profiles between layers with and without a velocity gradient. Travel times for the isovelocity case marked by dots; gradient case marked by open triangles . . . . .	42
8a	Plot of errors in determinations of velocity gradient. Absolute value of relative error is plotted against $\sigma_N/T_o$ , where $\sigma_N$ is the computed standard deviation of timing errors and $T_o$ is the vertical one-way travel time in $o$ the layer. Error bars represent two standard deviations of points between successive tick marks . . . . .	44
8b	Plot of errors in determinations of velocity (see Figure 8a) . . . . .	46

List of Figures (Cont.)

Figure		Page
9	Velocity structure and ray paths for model from Naini and Leyden (1973). Rays traced from $\theta_o = 20^\circ$ to $\theta_o = 85^\circ$ . Dashed line indicates solution when travel time curve from layer 4 is ignored. That the ray path do not appear to be circular is an artifact of the computer program; the program computes critical points for each ray (i.e. point of turnover or reflection and points of entry into layers) and connects them with straight lines . . . . .	50
10	Velocity structure and ray paths for model from Maynard (1973). Rays traced for $\theta_o = 30^\circ$ to $\theta_o = 85^\circ$ . . . . .	55

## I. INTRODUCTION

The purpose of this thesis is to investigate the application of a non-linear, least squares regression procedure to the analysis of seismic travel time data. The procedure is applied under the assumption of a horizontally layered model, with a linear velocity gradient in each layer. Solutions for the three layer parameters, velocity at the top of the layer velocity gradient, and thickness, provide a more detailed determination of the velocity-depth function than has previously been possible.

The layered model described above is particularly well-suited to the unconsolidated and semi-consolidated marine sediments (Layer 1 of the oceanic crust). Various investigations (Knox, 1965; Houtz et al., 1968; Hamilton, et al., 1974) have shown substantial velocity gradients in the sediments near the water-sediment interface; the magnitude of the gradient decreases with depth and is generally assumed to vanish at or near the top of the basaltic layer (Layer 2). The method presented here has been developed to deal specifically with the detailed velocity structure of Layer 1 rather than the gross structure of the oceanic crust.

Determinations of the velocity-depth function are of interest in several areas of investigation. The layer parameters are sought as descriptors of the sediment them-

selves. Efforts have been made (Hamilton, 1965, 1970; Naini and Leyden, 1973; Hamilton et al., 1974) to correlate velocities, velocity gradients, and thicknesses with factors such as sediment type, mode of origin, porosity, degree of lithification, and sedimentation rate.

The velocity-depth function is also important in acoustic propagation problems. In the case of low frequency (less than approximately 20 Hz) and long range, the propagation of sound in the ocean involves not only the water column but also the sea-floor sediments. An accurate knowledge of the velocity structure, including velocity gradients, will be necessary for the successful application of a general propagation theory.

#### Previous Approaches

The  $T^2-X^2$  method for reflection data has long been the standard for investigating the sediment layer. This approach was first formalized by Green (1938) and later expanded upon by Dix (1955) and Le Pichon et al. (1968), among others. The use of reflection rather than head wave refraction data is dictated by the physical nature of the sediment column. Clay and Rona (1965) have shown that the upper few hundred meters of Layer 1 have a complex structure of very thin layers. The acoustic impedance contrast between these layers is low and velocity reversals are common. For these reasons, head wave refractions from interfaces within Layer 1 are rarely observed.

Dix's (1955) major contribution was to demonstrate how the reflection travel time curve from any layer in a multi-layer model could be reduced to the equivalent single layer case if the overlying layers were already known. The Dix reduction is not exact in that it requires an asymptotic approximation to the travel time curve. The method presented below requires the same reduction, but, by using the parametric travel time equations (cf. Le Pichon et al., 1968), it can be accomplished in a more precise manner.

Since the  $T^2-X^2$  approach solves only for the velocity and thickness of a layer, other methods, (e.g. as described by Ewing and Nafe, 1963) have been employed to determine local velocity gradients. Most investigators (Knox, 1965; Houtz et al., 1968; Maynard, 1973; Hamilton, et al., 1974) instead make gradient determinations on a regional basis. A large number of independent reflection records are taken over a specified area. The layer velocity and thickness are determined by the Dix method as modified by Le Pichon et al. (1968). The velocities are plotted as a function of depth (in time or distance) and a least squares curve is determined. In many cases, the sediment velocity at the sea floor is constrained to the regional value given by Fry and Raitt (1961).

The non-linear least squares method than provides a more consolidated approach to the problem. The velocity gradients can be determined directly from the travel time

data on individual records, and thus can be specified locally. The procedure, in addition, computes limits on the accuracy of all parameter estimates.

#### Other Investigations with the Parametric Equations

At the outset of this investigation, it was hoped that the parametric travel time equations could be employed to solve for the degree of horizontal/vertical anisotropy within a layer. As detailed in Appendix A, it was found that for the case of elliptical anisotropy, such a solution was impossible. If one accepts the elliptical anisotropy model, this rather surprising result has disturbing implications regarding the accuracy of many previous thickness determinations. Kroenke (personal communication, 1974) has observed anisotropies of 5-10% in laboratory measurements on sediments from the Ontong-Java Plateau (DSDP Leg 30, Site 289). That degree of anisotropy could produce the same percentage error in seismic thickness solutions.

It was also found that the parametric equations could provide a fast and simple method for the solution of the isovelocity reflection case (Appendix B). This development is of considerable use in removing the effects of the water column, which has a very small velocity gradient.

## II. THE PARAMETRIC EQUATIONS

### The General Integrals

The parametric travel time equations will now be developed for ray paths in a single layer with a linear velocity gradient. The same equations have been derived by Slotnick (1959), by approaching the limit of infinitesimally thin isovelocity layers. An alternate approach using Fermat's principle of extremal time is possible. Since Fermat's principle is central to ray theory, the alternate approach is somewhat more elegant and is presented below.

Consider an isotropic half-space, within which seismic velocity varies linearly with depth (Figure 1). Taking coordinate axes at the upper surface ( $z$  axis positive downward), the velocity at  $z=0$  is  $b$  and the variation of velocity with depth is given by  $v = b + \gamma z$  where  $\gamma$  is the velocity gradient.

Consider now two arbitrary points, A and B, within the half-space. The travel time between A and B is given by the integral,

$$T = \int_A^B \frac{ds}{v} \quad (1)$$

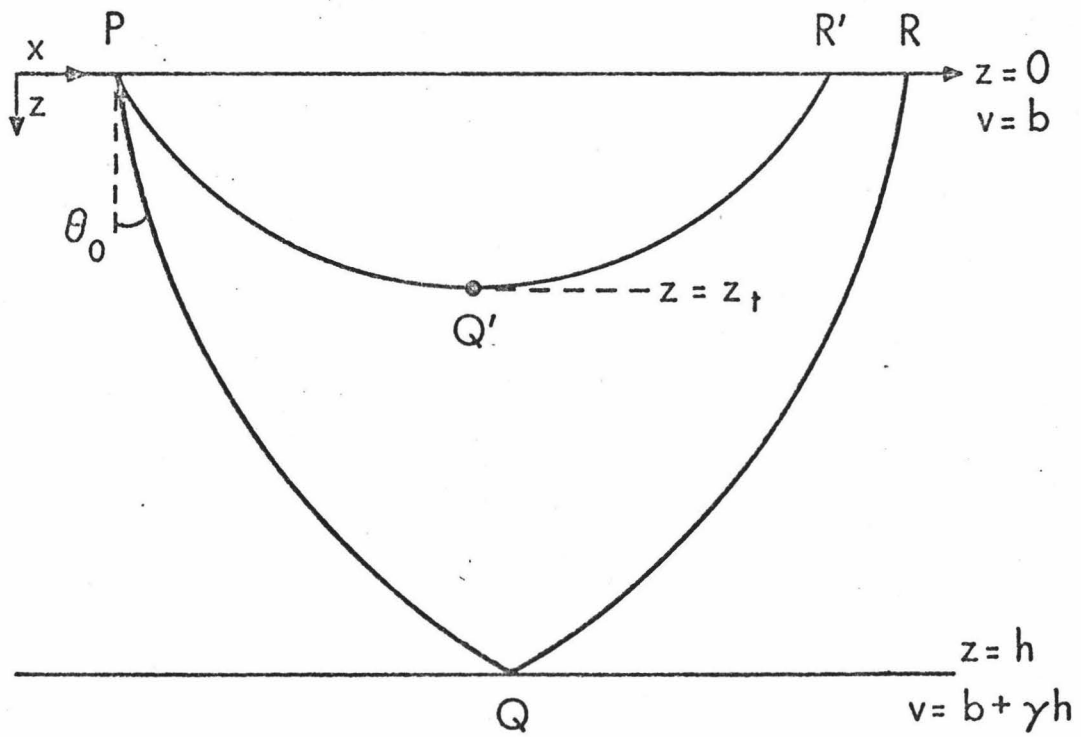
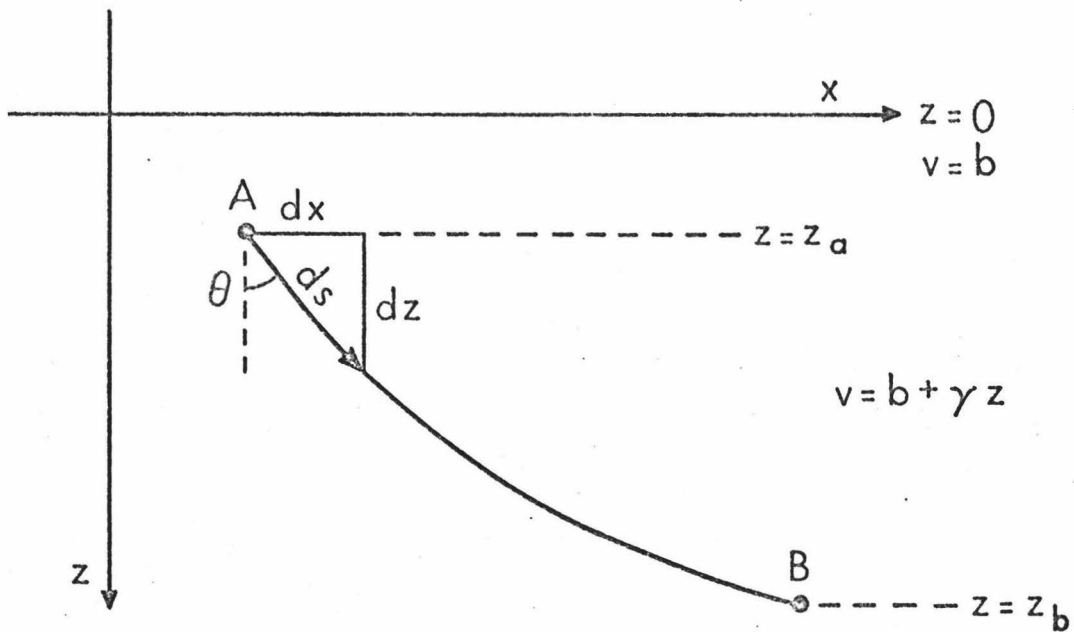
where  $ds^2 = dx^2 + dz^2$  and  $v = b + \gamma z$ .

Fermat's principle states that energy will travel between A and B along the path for which  $T$  is a minimum.

6.

Figure 1. General ray path in a half-space with a linear increase of velocity with depth.

Figure 2. Reflection (PQR) and refraction (PQ'R') ray paths in a layer with a linear velocity gradient.



Letting  $\dot{x} = dx/dz$ ,

$$ds = (1 + \dot{x}^2)^{1/2} dz$$

and equation 1 can be rewritten,

$$T = \int_{z_a}^{z_b} \frac{(1 + \dot{x}^2)^{1/2}}{b + \gamma z} dz = \int_{z_a}^{z_b} f(\dot{x}, z) dz \quad (2)$$

where  $z_a$  and  $z_b$  are the  $z$  coordinates of points A and B.

Examining equation 2, it is apparent that the integral  $T$  is now in the proper form to be minimized by using the calculus of variations. In the calculus of variations, it is assumed that the limits  $z_a$  and  $z_b$  are fixed but the path of integration is to be determined; that is, the ray path  $x = x(z)$  is unknown. From this relationship will come the parametric travel distance equation.

For  $T$  to be an extremum (in this case, a minimum) the partial differential equation,

$$\frac{\partial f}{\partial x} - \frac{d}{dz} \left( \frac{\partial f}{\partial \dot{x}} \right) = 0 \quad (3)$$

must be satisfied.

Substituting for  $f$  from equation 2 and noting that  $\frac{\partial f}{\partial x} = 0$ , equation 3 becomes

$$\frac{\partial f}{\partial \dot{x}} = \frac{1}{b + \gamma z} \frac{\dot{x}}{(1 + \dot{x}^2)^{1/2}} = \text{constant} \quad (4)$$

From Figure 1, it can be seen that the angle between the vertical and the tangent to the ray path is given by

$$\theta = \arctan \dot{x}$$

Thus

$$\frac{\dot{x}}{(1 + \dot{x}^2)^{1/2}} = \frac{\tan \theta}{\sec \theta} = \sin \theta$$

and it is clear that equation 4 is simply a statement of Snell's Law;

$$\frac{\sin \theta}{b + \gamma z} = \frac{\sin \theta}{v} = p \quad (5)$$

where  $p$  = constant for a particular ray path and is referred to as the ray parameter.

We now rewrite equation 4, replacing the right hand with  $p$ , squaring both sides and rearranging terms to get,

$$\dot{x}^2 = (b + \gamma z)^2 (1 + \dot{x}^2) p^2$$

or

$$\frac{dx}{dz} = \frac{p (b + \gamma z)}{[1 - (b + \gamma z)^2 p^2]^{1/2}} \quad (6)$$

To calculate the range,  $x$ , traversed along a ray path from depth  $z_a$  to depth  $z_b$  one need only rearrange equation 6 and integrate between the proper limits,

$$x = \int_{z_a}^{z_b} \frac{p (b + \gamma z)}{[1 - (b + \gamma z)^2 p^2]^{1/2}} dz \quad (7)$$

Note that if  $x$  is specified as the horizontal separation of points A and B, equation 7 can be solved for the ray parameter of the direct ray which connects the two points. Conversely, if a particular ray is specified, equation 7 will obviously yield the horizontal travel distance. Note also that the ray paths described by equation 7 are arcs of a circle (Slotnick, 1959, p. 208).

Equation 7 is one of two parametric equations which together will determine the surface travel time - distance curve when appropriate limits are applied. A similar equation will be derived for the travel time. At this point, however, it is convenient to make a change of variable in order to simplify the integration.

Let  $\phi = p(b + \gamma z)$ , from which,  $dz = d\phi/p\gamma$ .

Equation 7 then becomes,

$$x = \frac{1}{p\gamma} \int_{\phi_b}^{\phi_b} \frac{\phi}{(1-\phi^2)^{1/2}} d\phi \quad (8)$$

To develop the equation for the travel time,  $t$ , make the same change of variable in Equation 2. Then,

$$t = \int_{\phi_a}^{\phi_b} \frac{(1 + \dot{x}^2)^{1/2}}{(\phi/p)} \cdot \frac{d\phi}{p\gamma} \quad (9)$$

Note that from equation 5 and the definition of  $\phi$  that

$$\dot{x}^2 = \phi^2/1-\phi^2$$

so that equation 9 becomes

$$t = \frac{1}{\gamma} \int_{\phi_a}^{\phi_b} \frac{d\phi}{\phi(1-\phi^2)^{1/2}} \quad (10)$$

We will now investigate two choices of limits for equations 8 and 10.

Consider now the case of a single layer; a lower boundary is imposed on the half-space at  $z = h$  (Figure 2). We will take the shot point to be at the origin and consider rays in the region  $x \geq 0$ .  $\theta_0$  is the angle between the vertical and the tangent to an arbitrary ray at the origin. Note that each ray leaving the shot point has associated with it a unique ray parameter,  $p$ , corresponding to its initial angle  $\theta_0$ :  $p = \sin \theta_0 / b$ . The range  $0 \leq p \leq 1/b$  describes all rays possible for a given layer.

### Reflections

We will now compute the travel time and distance for the ray path PQR (Figure 2) which reflects from the lower interface. The ray path extends from  $z = 0$  to  $z = h$ , which corresponds to limits  $\phi = pb$  to  $\phi = p(b + \gamma h)$  in equations 8 and 10.

From equation 8

$$\begin{aligned} x &= \frac{1}{p\gamma} \int_{pb}^{p(b+\gamma h)} \frac{\phi}{(1-\phi^2)^{1/2}} d\phi \\ &= -\frac{1}{p\gamma} \left[ (1-\phi^2)^{1/2} \right]_{pb}^{p(b+\gamma h)} \end{aligned}$$

$$= \frac{1}{p\gamma} \left[ (1-p^2 b^2)^{1/2} - (1-p^2 (b+\gamma h)^2)^{1/2} \right] \quad (11)$$

and from equation 10

$$\begin{aligned} t &= \frac{1}{\gamma} \int_{pb}^{p(b+\gamma h)} \frac{d\phi}{\phi(1-\phi^2)^{1/2}} \\ &= -\frac{1}{\gamma} \left[ \ln \left( \frac{1+(1-\phi^2)^{1/2}}{\phi} \right) \right]_{pb}^{p(b+\gamma h)} \\ &= \frac{1}{\gamma} \left[ \ln \left( \frac{1+(1-p^2 b^2)^{1/2}}{pb} \right) \right. \\ &\quad \left. - \ln \left( \frac{1+(1-p^2 (b+\gamma h)^2)^{1/2}}{p(b+\gamma h)} \right) \right] \quad (12) \end{aligned}$$

We assume without proof that the ray path QR is identical to PQ so that the time and distance at the surface are double the  $x$  and  $t$  given by equations 11 and 12. The notation can be simplified by introducing

$$\beta = b+\gamma h$$

from the velocity at the bottom of the layer. Thus, the parametric equations which describe the reflection travel time curve at the layer surface are

$$x = \frac{2}{p\gamma} \left[ (1-p^2 b^2)^{1/2} - (1-p^2 \beta^2)^{1/2} \right] \quad (13a)$$

and

$$t = \frac{2}{\gamma} \ln \left[ \frac{\beta}{b} \frac{1+(1-p^2 b^2)^{1/2}}{1+(1-p^2 \beta^2)^{1/2}} \right] \quad (13b)$$

There is a restriction on the application of equations 13a and 13b. They are valid only in the range  $0 \leq p \leq 1/\beta$ . The ray  $p = 1/\beta$  just grazes the lower interface, i.e.  $\theta = \pi/2$  at  $z = h$ . Rays for which  $p > 1/\beta$  are totally refracted above the interface and are considered below.

#### Refractions

The ray path PQ'R' shown in Figure 2 is called a total internal refraction to distinguish it from the so-called head wave. The PQ'R' ray path "turns over" in the layer; that is,  $\theta = \pi/2$  for some  $z < h$ . In order to compute the surface travel time curve, one need only modify the upper limit of integration used in equations 11 and 12.

Instead of integrating down to  $z = h$ , the integration is carried only to the depth at which the ray turns over,  $z_t$ . Then, for the upper limit,

$$\phi = p(b + \gamma z_t)$$

but  $p = \sin \theta / v = \sin \frac{\pi}{2} / (b + \gamma z_t)$

since  $\theta = \pi/2$  at  $z = z_t$ .

Thus,  $\phi = 1$ .

Equations 8 and 10 then become,

$$x = \frac{1}{p\gamma} \int_{pb}^1 \frac{\phi}{(1-\phi^2)^{1/2}} d\phi = \frac{(1-p^2b^2)^{1/2}}{p\gamma} \quad (14a)$$

and

$$t = \frac{1}{\gamma} \int_{pb}^1 \frac{d\phi}{\phi(1-\phi^2)^{1/2}} = \frac{1}{\gamma} \ln \left( \frac{1+(1-p^2b^2)^{1/2}}{pb} \right) \quad (14b)$$

Again assuming  $Q'$  to be the midpoint in time and distance, the parametric equations become,

$$x = \frac{2}{p\gamma} (1-p^2b^2)^{1/2} \quad (15a)$$

$$t = \frac{2}{\gamma} \ln \left( \frac{1+(1-p^2b^2)^{1/2}}{pb} \right) \quad (15b)$$

which are valid in the range  $1/\beta \leq p \leq \frac{1}{b}$ .

#### Extension to the Multi-Layer Case

Following Slotnick (1959), the extension to the multi-layer case is straight-forward. Since the ray parameter is constant over any given ray path (equation 5), the total time and distance that a particular ray spans at the surface is simply the sum of the times and distances covered in the layers through which the ray passed.

Thus, the reflection travel time curve for reflections from the bottom of the  $n^{\text{th}}$  layer (Figure 3a) can be expressed (from equations 13a and 13b) as,

$$x = 2 \sum_{j=1}^n \frac{1}{p\gamma_j} \left[ (1-p^2 b_j^2)^{1/2} - (1-p^2 \beta_j^2)^{1/2} \right] \quad (16)$$

$$t = 2 \sum_{j=1}^n \frac{1}{\gamma_j} \ln \left[ \frac{\beta_j}{b_j} \frac{1+(1-p^2 b_j^2)^{1/2}}{1+(1-p^2 \beta_j^2)^{1/2}} \right]$$

where  $x$  and  $t$  are the distance and time,

$\gamma_j$  = velocity gradient of the  $j^{\text{th}}$  layer,

$b_j$  = velocity at the upper boundary of the  $j^{\text{th}}$  layer,

$\beta_j$  = velocity at the lower boundary of the  $j^{\text{th}}$  layer.

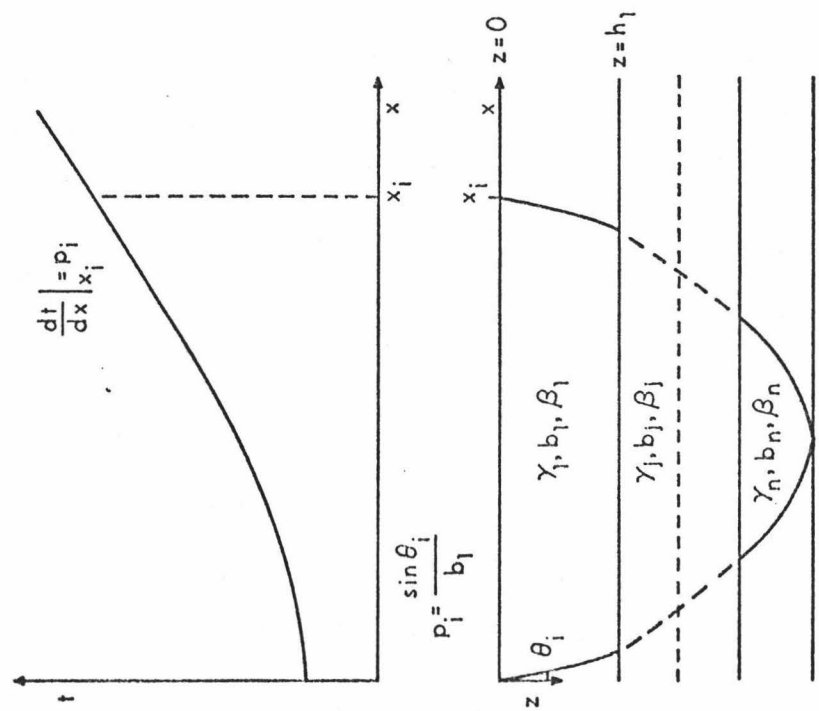
Following a similar argument, the travel time equations for the rays totally refracted in the  $n^{\text{th}}$  layer are written as the sum of the "reflection" ray paths in layers 1 to  $n-1$  and the refraction ray path in layer  $n$  (Figure 3b). That is, (from equations 13a and 13b and 15a and 15b),

$$x = 2 \sum_{j=1}^{n-1} \frac{1}{p\gamma_j} \left[ (1-p^2 b_j^2)^{1/2} - (1-p^2 \beta_j^2)^{1/2} \right] + \frac{2}{p\gamma_n} (1-p^2 b_n^2)^{1/2}$$

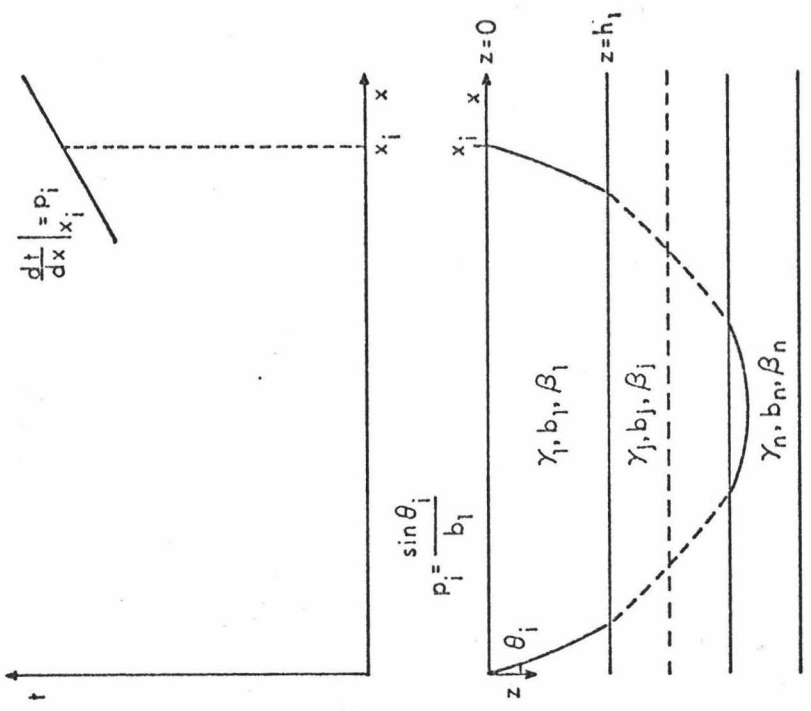
Figure 3

(a) Reflection ray path and travel time curve--  
multi-layer case.

(b) Total internal refraction ray path and travel  
time curve--multi-layer case.



(a)



(b)

(17)

$$t = 2 \sum_{j=1}^{n-1} \frac{1}{\gamma_j} \ln \left[ \frac{\beta_j}{b_j} \frac{1+(1-p^2 b_j^2)^{1/2}}{1+(1-p^2 \beta_j^2)^{1/2}} \right] + \frac{2}{\gamma_n} \ln \left[ \frac{1+(1-p^2 b_n^2)^{1/2}}{p b_n} \right]$$

### Slope of the Travel Time Curve

Finally, it is worthwhile to note an additional property of the ray parameter,  $p$ . If we differentiate equations 13a and 13b with respect to  $p$  and then divide 13b by 13a, it is easy to show that,

$$dt/dx = p \quad (18)$$

The same operations applied to equations 15a and 15b produce the same result. The linear nature of the differentiation operator makes it plain that the result also holds for the multi-layer cases.

The implications of equation 18 are important: the slope of the travel time curve at a given range,  $x$ , is equal to the ray parameter of the ray which emerges at this point (Figures 3a and b). The result holds regardless of the number of layers or whether the ray was reflected or totally refracted. This fact will be of central importance in correcting the travel time curves for the effects of overlying layers.

### III. SOLUTION OF THE PARAMETRIC EQUATIONS

Consider now the inverse of the problem presented in Section II; that is, given the surface travel time curves from  $n$  layers, solve for the velocity, velocity gradient, and thickness of each.

As in the standard methods of interval velocity analysis, the parameters are solved for successively from the top layer downward. Each travel time curve is then reduced to the single layer case by applying the results from overlying layers. The solution of the  $n$  single layer cases will be accomplished by fitting the theoretical curves from Section II to the observed data. The "best" fit will be determined by the least squares criterion. The nature of confidence regions about the solution will also be investigated.

#### Method

##### 1. Removal of effects from overlying layers.

Assume that solutions have been made for the parameters of layers 1 through  $n-1$  and consider the travel time curve for reflections from the base of layer  $n$ . Additionally, assume that the tangent to the travel time curve is known at all points. Using equations 16, the travel time and distance in the  $n^{\text{th}}$  layer can be written as,

$$x^R = x^{-2} \sum_{j=1}^{n-1} \frac{1}{p\gamma_j} \left[ (1-p^2 b_j^2)^{1/2} - (1-p^2 \beta_j^2)^{1/2} \right] \quad (19)$$

$$t^R = t^{-2} \sum_{j=1}^{n-1} \frac{1}{\gamma_j} \ln \left[ \frac{\beta_j}{b_j} \frac{1+(1-p^2 b_j^2)^{1/2}}{1+(1-p^2 \beta_j^2)^{1/2}} \right]$$

where the R superscript refers to reduced distance and time.

Since  $p$  is known over the whole travel time curve, it is evident that  $(x^R, t^R)$  can be computed exactly from any  $(x, t)$ .

In practical applications, one does not have a continuous travel time curve but rather a set of observations,  $\{(x_i, t_i), i=1, 2, \dots, m\}$ , from it. Since equations 19 are valid for arbitrary  $(x, t)$  they are valid for all  $(x_i, t_i)$ . Since the  $(x_i, t_i)$  are discrete, however, no derivative is defined. Consequently, the ray parameter at each point must be estimated.

A satisfactory estimate can be made by fitting a least squares polynomial to the set of points  $(x_i, t_i)$ . Then  $p_i$ , the ray parameter at  $x = x_i$  is given from equation 18,

$$p_i = (d\tau/dx)_{x=x_i} \quad (20)$$

where  $d\tau/dx$  is the derivative of the polynomial.

Thus for any set of travel time and distance points  $(x_i, t_i)$  one can construct a set of reduced points  $(x_i^R, t_i^R)$  from equation 19 simply by replacing  $x$  by  $x_i$ ,  $t$  by  $t_i$ , and  $p$  by  $p_i$ . The reduced points can now be used to solve the single layer equations. Note that the procedure for reducing the multi-layer refraction travel time curve is exactly the same.

## 2. The sum of squares function.

We now wish to fit one of the theoretical models developed in Section II to a given set of reduced observed data. Since any set of observed data is subject to random errors, least squares will be used to determine the best fitting model. Thus we seek to minimize,

$$E(\gamma, b, \beta) = \sum_{i=1}^m (Y_i - \hat{Y}(W_i, \gamma, b, \beta))^2 \quad (21)$$

where  $(Y_i, W_i)$  is one observation pair of a reduced travel time curve and  $\hat{Y}(W_i, \gamma, b, \beta)$  is a predicted value of  $Y_i$  based on the parameters of the model and the observation  $W_i$ .

Equation 21 was deliberately expressed in terms of a general observation pair  $(Y_i, W_i)$  because there are three sets of observations, any two of which are sufficient to solve the problem. In addition to time and distance, there is the set of ray parameters,  $p_i$ . The theoretical

models developed in equations 13 and 15 already relate  $x$  to  $p$  and  $t$  to  $p$ . As will be shown below, a model is easily developed relating  $x$  to  $t$ . The choice of which pair of the three depends on what is mathematically most convenient.

### Reflections

For the case of reflections we will minimize the sum of squares function,

$$E(\gamma, b, \beta) = \sum_{i=1}^m \left( x_i - \frac{2}{p_i \gamma} \left[ (1 - p_i^2 b^2)^{1/2} - (1 - p_i^2 \beta^2)^{1/2} \right] \right)^2 \quad (22)$$

where  $x_i$  is reduced observed travel distance and

$p_i$  is the ray parameter at  $x = x_i$ .

The model (equation 13a) was chosen in terms of  $(x_i, p_i)$  pairs because the procedure for minimizing  $E$  involves differentiation with respect to  $\gamma$ ,  $b$ , and  $\beta$ . Equation 13b, relating  $t$  and  $p$ , provides a model much more difficult to differentiate. The model directly relating  $x$  and  $t$  is more cumbersome still.

### Refractions

For the refraction case, it is more convenient to use the relation between  $x$  and  $t$ . The desired relation can be obtained by eliminating the ray parameter,  $p$ , from

equations 15. From Slotnick (1959),

$$x = \frac{2b}{\gamma} \sinh \left( \frac{\gamma t}{2} \right) \quad (23)$$

for the theoretical single layer refraction. The sum of squares then becomes, in the single layer case,

$$E(\gamma, b) = \sum_{i=1}^m \left( x_i - \frac{2b}{\gamma} \sinh \left( \frac{\gamma t_i}{2} \right) \right)^2 \quad (24)$$

At this point it is essential to note that the refraction travel time curve does not contain enough information to completely solve the problem at hand. Minimizing  $E(\gamma, b)$  will provide no information about the total thickness of the layer (or, equivalently, velocity at the bottom of the layer). This should not be surprising since the refraction ray paths never reach the bottom of the layer; they "know" nothing of its existence.

To remedy this situation an independent piece of data must be introduced. The vertical one-way travel time within the layer is sufficient. By setting  $p = 0$  (normal incidence) and rearranging equation 13b, it is simple to show that,

$$h = \frac{b}{\gamma} (e^{\gamma T_0} - 1) \quad (25)$$

where  $T_0$  is the one-way travel time.

The value of  $T_0$  is usually easy to determine from an ASPER (see Maynard et al., 1974) or normal incidence profiler record.

### 3. Minimization of the sum of squares.

In standard least squares problems the sum of squares function is minimized by first taking derivatives with respect to the parameters. Setting the derivatives to zero provides a set of  $N$  equations in  $N$  unknowns, where  $N$  is the number of parameters in the model. When the model is linear in the parameters, the normal equations are linear and easily solved. Equations 22 and 24 are both obviously non-linear in the parameters  $\gamma$ ,  $b$ , and  $\beta$ . The normal equations for this case are extremely complicated and unsolvable by exact analytical techniques.

To minimize the sum of squares function we employ an iterative, numerical approach first published by Davidon (1959) and later expanded upon by Fletcher and Powell (1965). The procedure was developed to find the local minimum of any function whose first partial derivatives can be expressed analytically. Consequently, the sum of squares,  $E$ , will be viewed simply as a function of the variables  $\gamma$  and  $b$  (equation 24) or  $\gamma$ ,  $b$ , and  $\beta$  (equation 22).

It is convenient to think of the sum of squares function as defining a surface in an  $N+1$  dimensional

space.  $N$  dimensions are defined by the  $N$  parameters of the model; this subspace is termed the parameter space. The other dimension corresponds to values of the sum of squares.

Davidon's method is iterative; given an arbitrary first approximation of the location of the minimum, a direction of search is determined. The direction is that of the gradient of the surface (the path of steepest descent) modified slightly in order to speed convergence. Along this direction of search the minimum of the function is determined, and this point becomes the new approximation. The procedure repeats until the change in the location of the minimum's between successive iterations is less than some specified amount. The minimum of the least squares function will be denoted in parameter space as  $(\hat{\gamma}, \hat{b}, \hat{\beta})$  or  $(\hat{\gamma}, \hat{b})$  and referred to as the least squares estimate of the parameter values.

Davidon's method has several advantages. First, Fletcher and Powell (1965) prove that convergence is assured if a local minimum exists. Second, convergence in the neighborhood of the minimum is swift. Third, the method yields the second partial derivatives of the function at the minimum; these, as shown in the next section, are useful in computing confidence regions. Finally, Davidon's method is presently implemented as a

FORTTRAN program in the IBM Scientific Subroutine Package  
(Version III, 1970).

#### 4. Confidence regions.

The  $\alpha\%$  confidence region for a given estimate is that locus of points in parameter space which have an  $\alpha\%$  probability of including the true answer. Having arrived at an estimate of the parameters for a layer, it is important to exhibit the confidence region to illustrate the possible error in the determination.

Beale (1960) defines the approximate  $\alpha\%$  confidence region as the set of points for which,

$$E - \hat{E} \leq N s^2 F_{\alpha} (N, m-N) \quad (26)$$

where  $\hat{E} = E(\hat{\gamma}, \hat{b}, \hat{\beta})$  or  $E(\hat{\gamma}, \hat{b})$

$s^2$  is an estimate of the variance of the  
experimental error

$m$  is the number of observations

$N$  is the number of parameters estimated

(2 or 3)

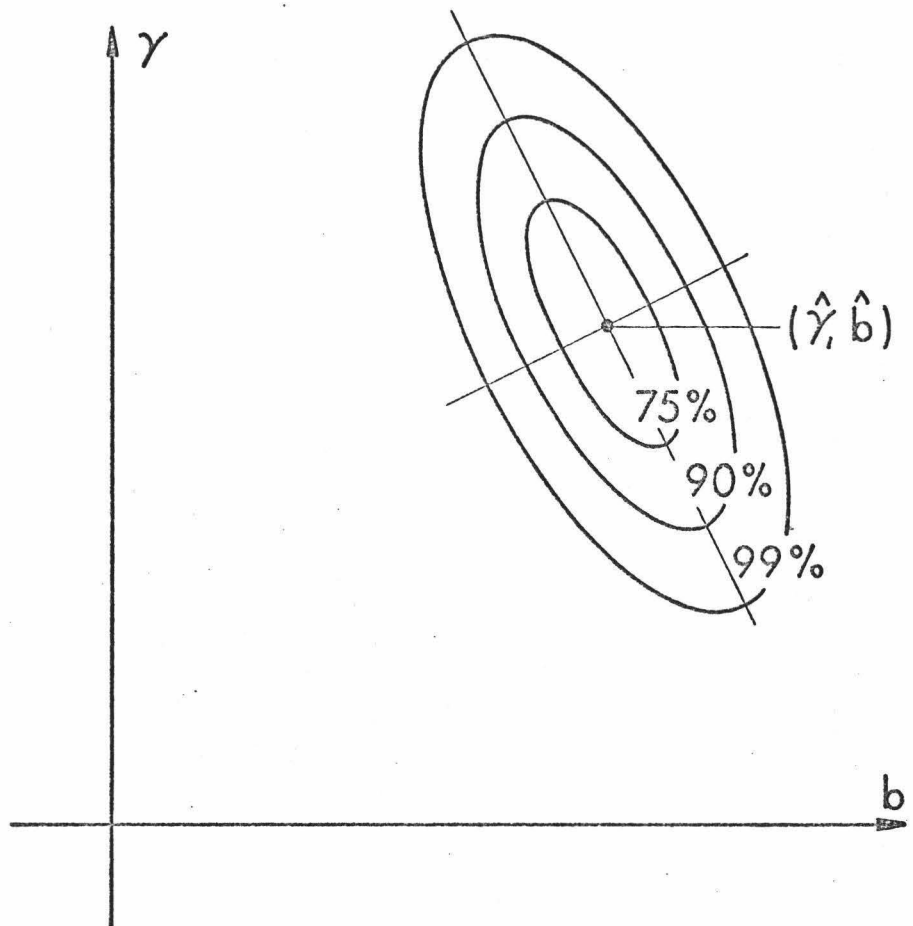
and  $F_{\alpha}(N, m-N)$  is the  $\alpha\%$  probability point of the  
 $F$  (variance ratio) distribution function with  
 $N$  and  $m-N$  degrees of freedom.

The confidence region defined by equation 26 will look something like it is shown in Figure 4. In Figure 4 the refraction case was assumed so that the parameter space is the  $\gamma$ - $b$  plane. The disparity in magnitude between the major and minor axes indicates that one parameter (in this case,  $\gamma$ ) is not as well determined as the other. The fact that the ellipse axes are not parallel to the coordinate axes indicates that the two parameters are not entirely independent. It is because of this dependence that the entire confidence region must be specified rather than merely confidence limits on each parameter.

Equation 26 is an adequate approximation to the exact confidence region only when the model is not too non-linear. Beale's  $N_0$  statistic, a measure of non-linearity, was computed for both the reflection and refraction cases. In both cases, the criterion (Beale, 1960, eqn. 4.3, p. 60) for satisfactory linearity was met by almost an order of magnitude. Equation 26 is then accurate within 2-3%.

Actually computing the confidence regions, however, can be quite time consuming. We therefore assume that the sum of squares function can be approximated satisfactorily in the neighborhood of  $(\hat{\gamma}, \hat{b})$  by a Taylor series expansion with second order terms. Following Beale (1960) and again using the refraction case,

Figure 4. Confidence regions about an estimate  $(\hat{\gamma}, \hat{b})$   
for  $\alpha = 75, 90$  and  $99\%$ .



$$\begin{aligned}
E(\gamma, b) &= E(\hat{\gamma}, \hat{b}) + E^{\hat{\gamma}} \Big|_{\hat{\gamma}} \Delta\gamma + E^b \Big|_{\hat{b}} \Delta b \\
&+ \frac{1}{2} \left[ E^{\gamma\gamma} \Delta\gamma^2 + 2E^{\gamma b} \Delta\gamma \Delta b \right. \\
&\quad \left. + E^{bb} \Delta b^2 \right]_{\hat{\gamma}, \hat{b}} \tag{27}
\end{aligned}$$

where  $E^{\gamma}$  and  $E^b$  equal  $\frac{\partial E}{\partial \gamma}$  and  $\frac{\partial E}{\partial b}$  respectively,

$$\begin{aligned}
E^{\gamma\gamma} &= \frac{\partial^2 E}{\partial \gamma^2} & E^{\gamma b} &= \frac{\partial^2 E}{\partial \gamma \partial b} & E^{bb} &= \frac{\partial^2 E}{\partial b^2} \\
\Delta\gamma &= \gamma - \hat{\gamma} & \text{and} & & \Delta b &= b - \hat{b}
\end{aligned}$$

Note also (Beale, 1960),

$$s^2 \approx \frac{\hat{E}}{m-N} = \frac{E(\hat{\gamma}, \hat{b})}{m-N} \tag{28}$$

The definition of the confidence region can be revised by substituting equations 27 and 28 into equation 26 and noting  $E^{\gamma} = E^b = 0$  and  $N = 2$ , so that,

$$\begin{aligned}
E^{\gamma\gamma} (\gamma - \hat{\gamma})^2 + 2E^{\gamma b} (\gamma - \hat{\gamma}) (b - \hat{b}) \\
+ E^{bb} (b - \hat{b})^2 \leq \frac{4 E(\hat{\gamma}, \hat{b})}{m-2} F_{\alpha} \tag{29}
\end{aligned}$$

The confidence region is now easily computed in the  $\gamma$ - $b$  plane by simply solving a quadratic equation at several points. The quantities  $E^{\gamma\gamma}$ ,  $E^{\gamma b}$ ,  $E^{bb}$ , and  $E(\hat{\gamma}, \hat{b})$  are, as previously mentioned, direct results of Davidon's method.

### Acceptance Regions

In order to evaluate the inaccuracies of the method we will now investigate the acceptance region corresponding to the defined confidence regions. We define a point in parameter space,  $(\gamma_T, b_T)$  which is the true value of the parameters. The  $\alpha\%$  acceptance region for  $(\gamma_T, b_T)$  is the locus of estimates  $(\hat{\gamma}, \hat{b})$  whose  $\alpha\%$  confidence regions include  $(\gamma_T, b_T)$ . That is, if the estimation of the true parameter values were performed a large number of times, the  $\alpha\%$  acceptance region defines that area in parameter space within which one would expect to find  $\alpha\%$  of the estimates.

In application of the estimation procedure to real data, it is desirable to have knowledge of the dependence of the acceptance region on pertinent experimental factors. With this knowledge it is possible to specify criteria for the experimental method (e.g. the requisite timing accuracy) in order to be reasonably sure that the estimation errors will be less than a certain magnitude.

Beale (1960) provides an analytical definition of the acceptance region, but the necessary computations are exceedingly difficult. For our purposes, an empirical estimate of the acceptance limits on each parameter will be sufficient. The following section describes model studies undertaken to provide this estimate.

Figure 5 is a flow chart of the computer program used to evaluate the problem. Details of the procedure are as follows:

1) Travel time curves were generated from a given set of layer parameters by equations 16 or 17. Table 1 shows the five different sets used. A typical set of layer parameters, displayed as a velocity-depth profile, is shown in Figure 6. As in all test models, the first layer is assumed to be an isovelocity water column ( $v = 1.5$  km/sec). The layers under the water column all have the same vertical one-way travel time (for the model in Fig. 6,  $T_0 = .12$  sec.) The gradient for each layer was chosen arbitrarily from the range  $0.2- 2.0$  sec<sup>-1</sup> and the velocity at the top of the layer was chosen so that there would be only small discontinuities (both positive and negative). With the information given above, the layer thickness was fixed by equation 25.

2) The effect of the water column was removed. Since an isovelocity approximation was found satisfactory, the water column was solved by the method described in Appendix B. It was found that the isovelocity solution was always accurate enough that it had no discernable effect on any solution for the lower layers. In later runs, therefore, the water column solution was simply assumed.

Figure 5. Flow chart of the computer program used to evaluate acceptance limits.

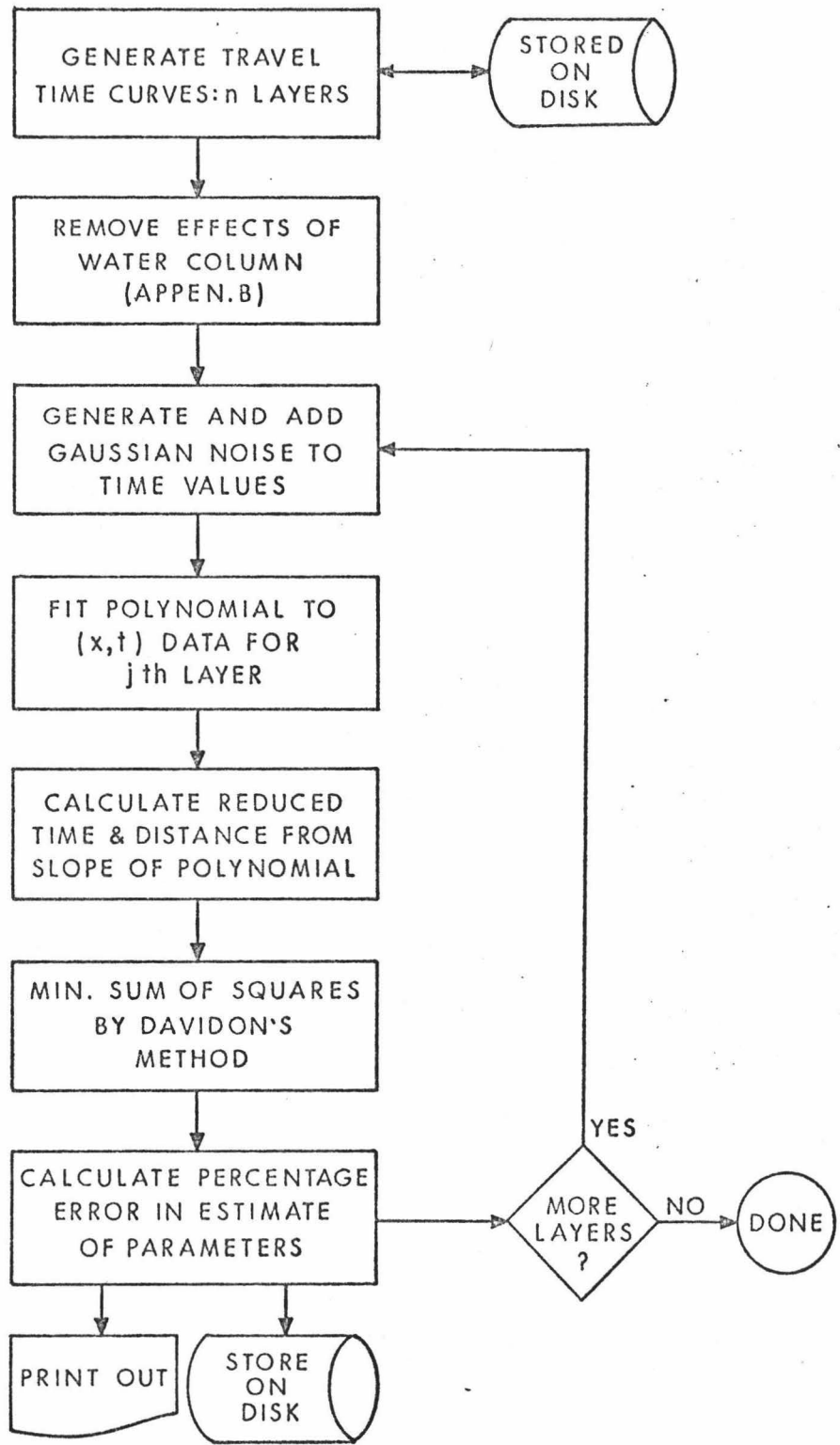


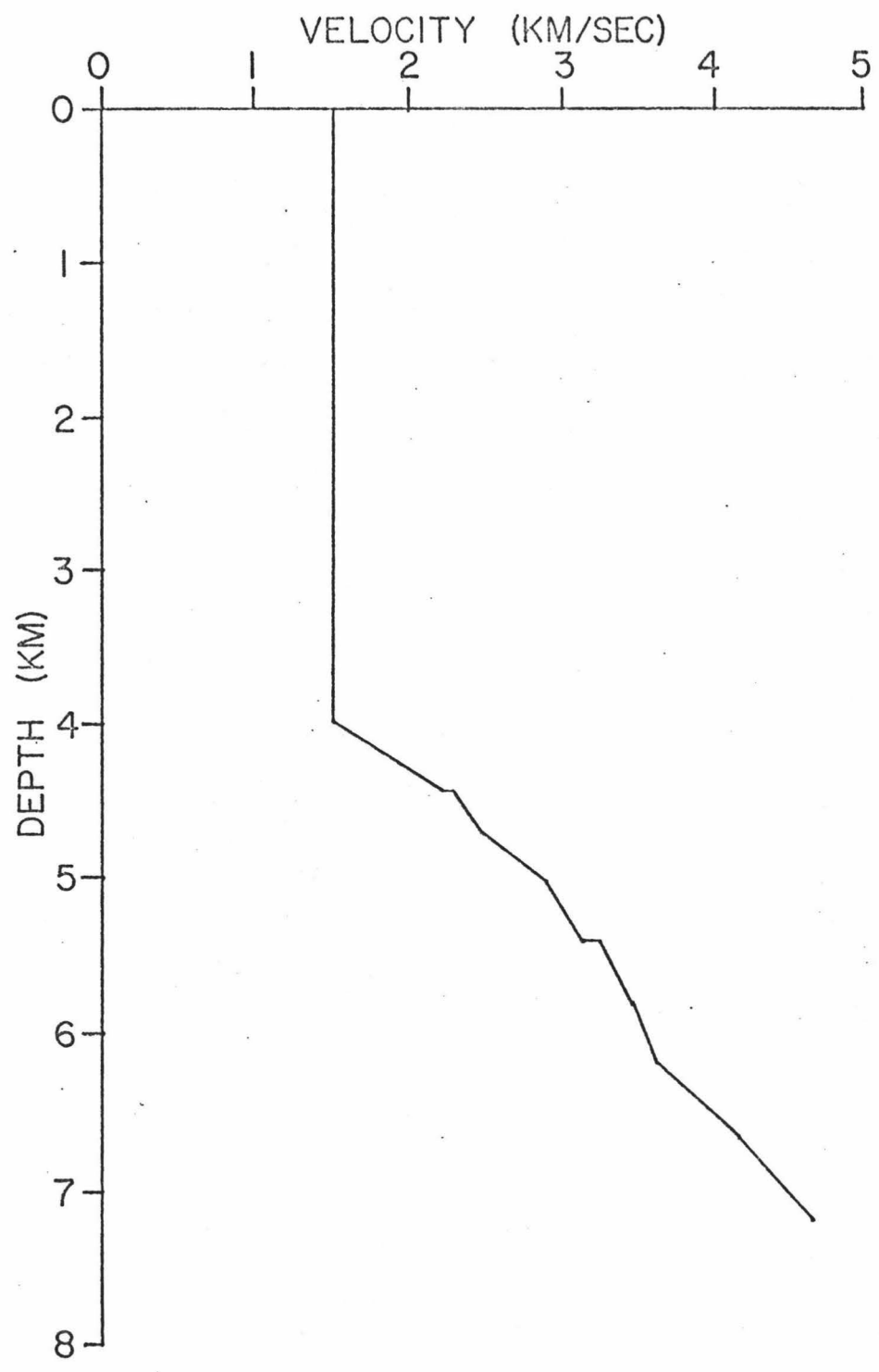
Table 1. The five parameter sets used to test the regression procedure. In every model, layer 1 is a water column ( $v = 1.5$  km/sec,  $h = 4.0$  km). Velocity gradients in  $\text{sec}^{-1}$ , velocities in km/sec and thicknesses in km.

Layer	Model 1 ( $T_o = .06$ sec)			Model 2 ( $T_o = .075$ sec)			Model 3 ( $T_o = .09$ sec)		
	$\gamma$	$b$	$h$	$\gamma$	$b$	$h$	$\gamma$	$b$	$h$
2	1.5	1.55	.097	1.9	1.51	.122	1.5	1.52	.146
3	1.2	1.71	.106	0.9	1.75	.136	1.4	1.74	.166
4	1.4	1.90	.119	1.7	1.90	.152	1.3	1.98	.189
5	0.7	2.07	.127	1.2	2.25	.177	1.2	2.23	.212
6	0.9	2.16	.133	0.6	2.47	.189	1.1	2.49	.235
7	1.1	2.35	.146	0.8	2.59	.200	1.0	2.75	.259
8	0.8	2.51	.154	0.5	2.80	.214	0.9	3.01	.282
9	1.3	2.64	.165	0.7	2.92	.225	0.8	3.27	.305
10	1.0	2.87	.177	1.0	3.10	.242	0.7	3.52	.327

Table 1 (continued)

Layer	Model 4 ( $T_o = .12$ sec)			Model 5 ( $T_o = .15$ sec)		
	$\gamma$	b	h	$\gamma$	b	h
2	1.7	1.50	.200	1.4	1.53	.255
3	1.6	1.84	.243	1.5	1.89	.318
4	0.7	2.30	.288	0.8	2.37	.378
5	1.2	2.51	.324	1.2	2.67	.439
6	0.6	2.92	.363	1.3	3.20	.530
7	0.5	3.25	.402	0.9	3.89	.625
8	0.4	3.46	.425	0.5	4.45	.693
9	1.1	3.65	.468	0.4	4.79	.740
10	0.9	4.17	.528	0.3	5.09	.781

Figure 6. Velocity-depth profile of typical test model  
( $T_0 = .12$  sec).



3) To a given set of  $t_i$  values, normally distributed random numbers were added to simulate random measurement errors. The standard deviation of the random errors,  $(\sigma_N)$  was computed and stored.

4) A polynomial was fit to the observations using least squares and the  $p_i$  were calculated (equation 20). In practice it was found that a polynomial of the form

$$t = a_0 + a_1 x^2 + a_2 x^4 \quad (30)$$

was sufficient to describe the data. Clay and Rona (1965) give a detailed justification for neglecting terms of odd order in the case of non-sloping layers. Note that the least squares polynomial has the additional effect of smoothing, tending to average out the random errors introduced in step 3. The number of terms used is a compromise between smoothing and adequately describing the data. Using the determinations of the  $p_i$ , the reduced observations were computed by equation 19.

5) The sum of squares function (equation 22 or 24) was minimized by Davidon's method. The parameter estimates were compared with the known values and the relative errors recorded.

6) The procedure returns to step 3 until all layers have been solved.

### Results

Trial and error with the above program indicated that as the magnitude of the timing errors increased, so did the maximum relative error in the parameter estimates. It was also noted that for a given standard deviation of timing error, the maximum relative error for thick layers was smaller than that for thinner ones. On the basis of these two results, it was decided to use the ratio  $\sigma_N/T_0$ , where  $\sigma_N$  is the standard deviation of the timing errors and  $T_0$  the vertical one-way travel time, as a variable to describe the behavior of the acceptance limits. It was hoped that the size of the acceptance limits would vary strongly with this ratio. The computer program was run with a large variety of layer parameters and error magnitudes in order to delineate this variation.

The results of this analysis for the case of reflections were disappointing. There was no combination of circumstances (except  $\sigma_N = 0$ ) which would ensure consistent estimates. Even with timing errors of extremely small magnitude, correlations among the random numbers would cause huge ( $\pm 100\%$ ) error in estimates of the gradient. Estimates of the velocity and thickness, however, were substantially better (at most  $\pm 15\%$  error).

This failure is not altogether surprising.

Le Pichon et al. (1968), in testing their interval velocity estimation procedure, note that the introduction of

velocity gradients of up to  $1.0 \text{ sec}^{-1}$  had no significant effect on their solutions. It is easy to demonstrate that the reflection travel time curve for a layer with a linear velocity gradient can be nearly identical to that for an isovelocity layer. Figure 7 shows various points on the travel time curves for a pair of two layer cases. In both cases, the first layer is an isovelocity water column ( $v = 1.5 \text{ km/s}$ ,  $h = 3.0 \text{ km}$ ). Both second layers are 300 m thick and have a time-average velocity of  $1.783 \text{ km/s}$ . In one case, however, the second layer is isovelocity ( $v = 1.783 \text{ km/s}$ ) and in the other it has a substantial gradient ( $\gamma = 2.0 \text{ sec}^{-1}$ ,  $b = 1.5 \text{ km/s}$ ).

Examination shows that the two travel time curves are virtually indistinguishable over their entire extent. At any given range, the difference in travel time is always less than 10 msec. This discrepancy is not large when compared to even low magnitude of timing error ( $\sigma_N = .001 \text{ sec}$  say) and therefore, estimates of the gradient will be poorly determined.

For refractions, the method is considerably more stable than for reflections. Figures 8a and 8b show the absolute value of relative error for gradient and velocity of all solutions made plotted against  $\sigma_N/T_0$ . The results are not surprising: in order to maintain comparable levels of precision, thin layers must be timed more accurately than thick ones.

Figure 7. Comparison of reflection travel time curves and velocity-depth profiles between layers with and without a velocity gradient. Travel times for the isovelocity case marked by dots; gradient case marked by open triangles.

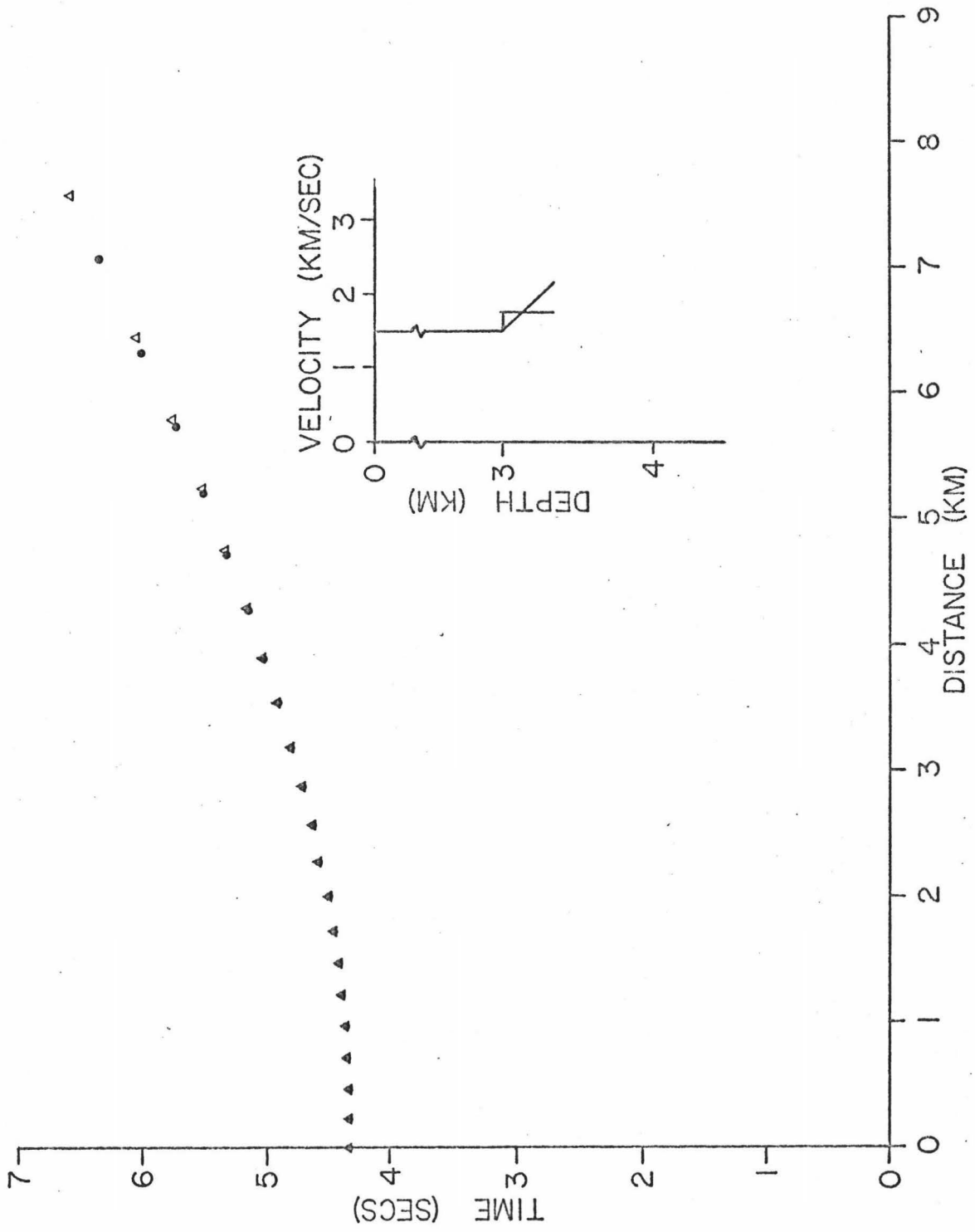


Figure 8.

- (a) Plot of errors in determinations of velocity gradient. Absolute value of relative error is plotted against  $\sigma_N/T_o$ , where  $\sigma_N$  is the computed standard deviation of timing errors and  $T_o$  is the vertical one-way travel time in the layer. Error bars represent two standard deviations of points between successive tick marks.

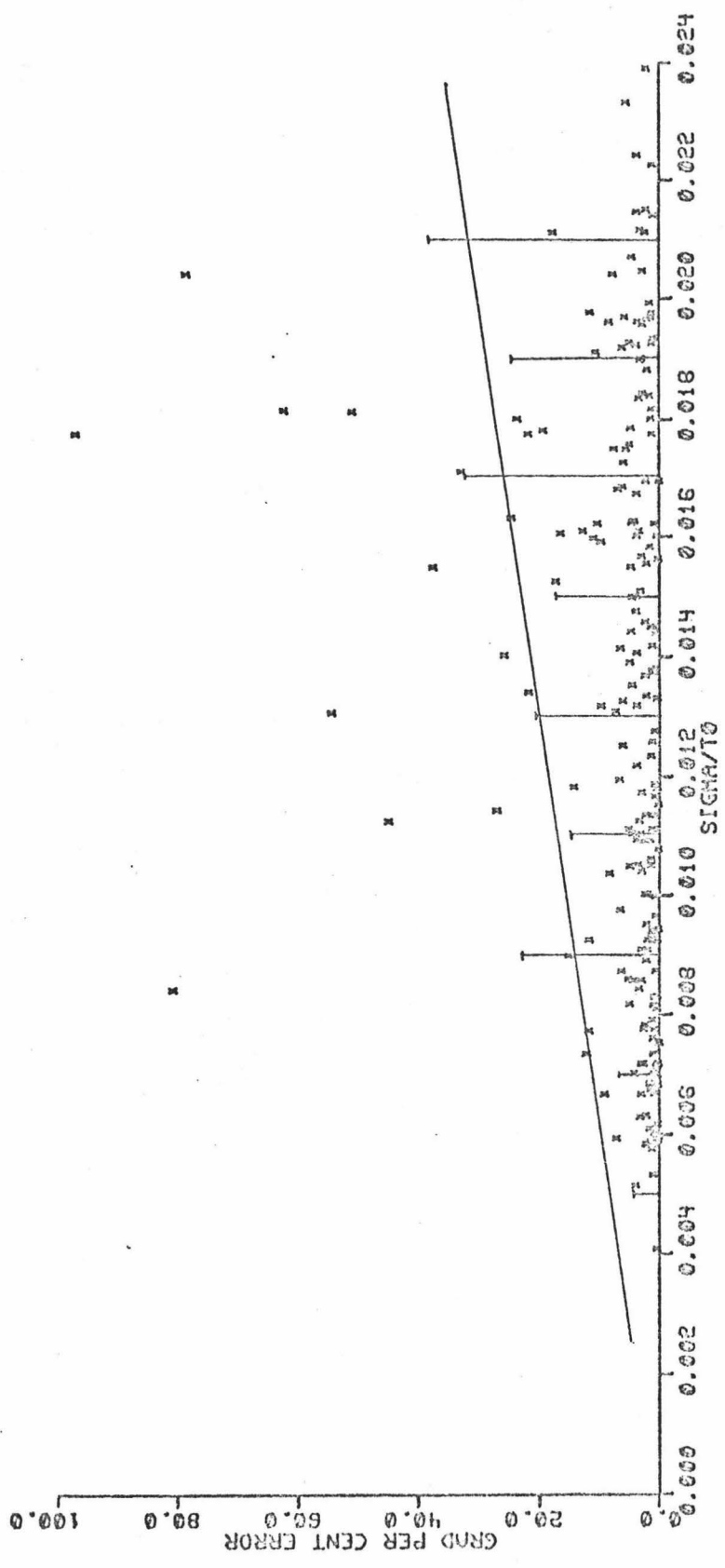
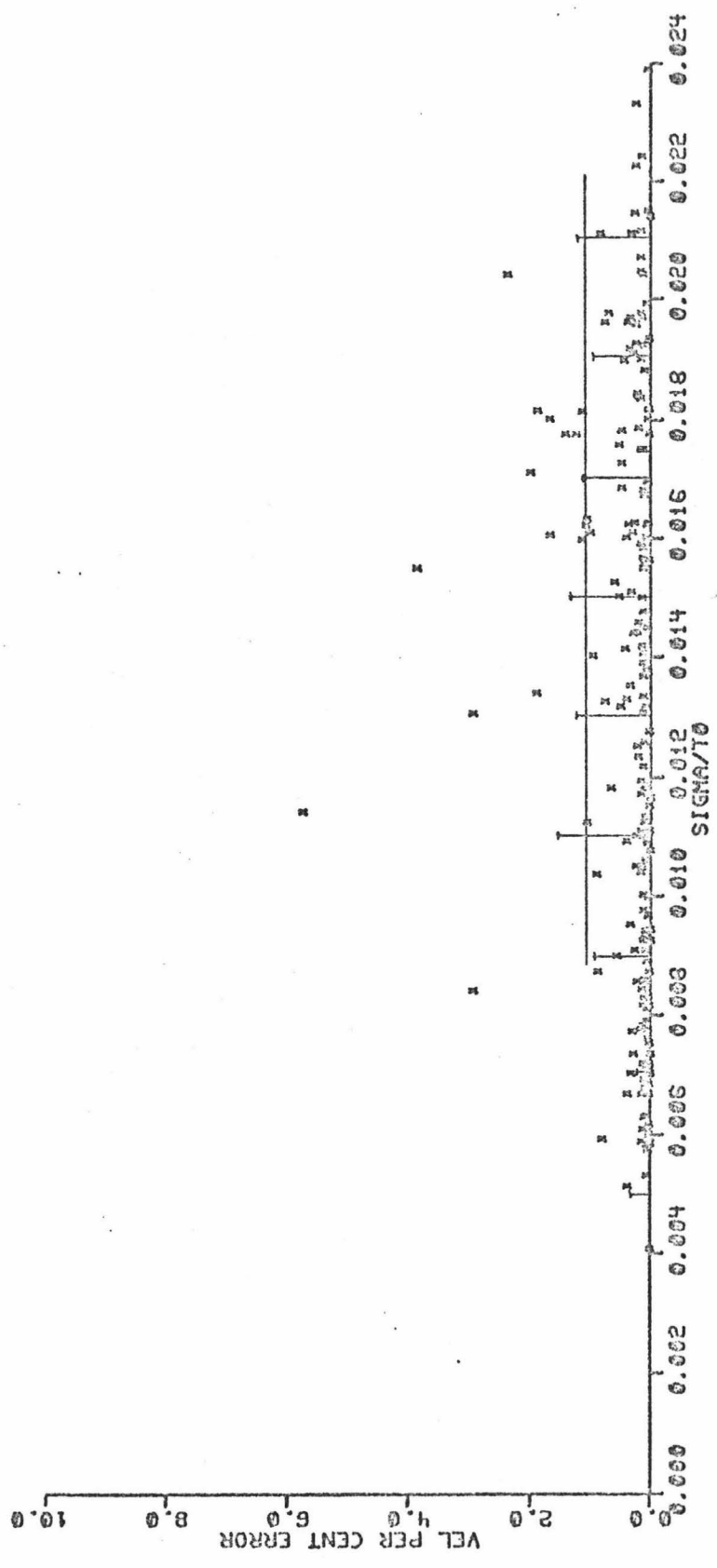


Figure 8.

(b) Plot of errors in determinations of velocity  
(see Figure 8a).



The bars on Figures 8a and 8b indicate two standard deviations of the errors between consecutive tick marks. The solid curve then is a rough estimate of the 95% acceptance limit for each parameter.

Notice that the gradient is considerably less well determined than the velocity. However, the gradient can be estimated with reasonable accuracy ( $\pm 20\%$ ) up to a  $\sigma_N/T_o$  ratio of about 0.014. For the determinations considered the velocity shows no appreciable trend after a jump at about  $\sigma_N/T_o = 0.008$ . Analysis of equation 25 will show that the 95% acceptance limit for thickness is similar to that for velocity.

This concludes the discussion of the inherent statistical limitations of the method. The next section will consider certain physical limitations and the problem of actually observing such refracted returns.

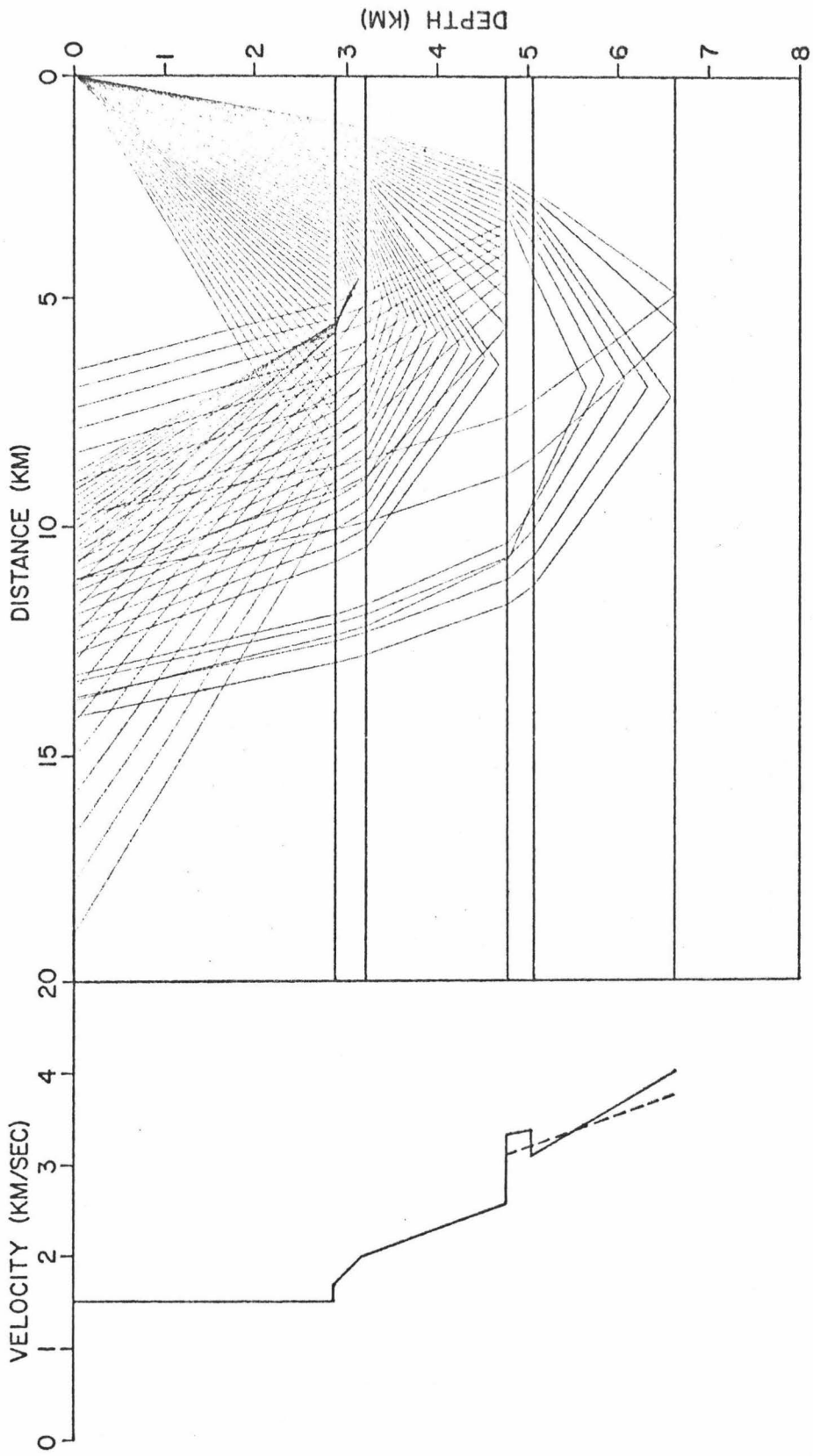
## IV. DISCUSSION AND CONCLUSIONS

Sections II and III have provided a firm theoretical basis for the analysis of refracted rays. The successful application of the method, however, hinges on the identification of such refracted returns in actual experiments. Maynard et al. (1974) present an extensive qualitative discussion on the nature of total internal refractions (often termed  $R_s$  rays). The authors exhibit theoretical travel time curves for several two layer cases, encompassing a wide variety of physical situations. In addition, several pitfalls and complications of the analysis of real data are examined in detail.

Using Maynard's theoretical travel time curves as a guide, a review was made of numerous ASPER records. Records from the Ontong-Java Plateau were examined most closely because in this area substantial velocity gradients were suspected to exist in almost perfectly non-sloping layers (Maynard, 1973). The findings were, unfortunately, entirely negative. At the expected times and distances any refracted arrivals present were totally obscured by noise or reflected arrivals from other layers.

The lack of real data leaves open the question of whether the method presented in this paper can be successfully applied. In an effort to resolve this question, a discussion of both the potential problems and advantages

Figure 9. Velocity structure and ray paths for model from Naini and Leyden (1973). Rays traced from  $\theta_o = 20^\circ$  to  $\theta_o = 85^\circ$ . Dashed line indicates solution when travel time curve from layer 4 is ignored. That the ray paths do not appear to be circular is an artifact of the computer program; the program computes critical points for each ray (i.e. point of turnover or reflection and points of entry into layers) and connects them with straight lines.



of the application of this method to the study of marine sediments is warranted. Whereas the model studies of Section III have investigated only the statistical limitations of the method, what follows will be primarily concerned with practical problems. We will illustrate some (certainly not all) of the physical limitations and comment on some possible improvements to the ASPER system. It should be emphasized that when the discussion is complete the question will not have been resolved. Only application will provide the answer; this discussion is undertaken to guide the experimenter.

The major potential problems in applying this  $R_s$  analysis to the study of marine sediments can be grouped in three categories: physical, general, and experimental. Following is a description and examples of each problem, along with the restrictions each imposes on the use of the method.

#### Physical problems

The first class of problems arises from the physical nature of the velocity structure of the sediment column. Two examples will be presented: the effect of irregularities in the velocity structure and the "bunching" of rays refracted in deep layers.

Figure 9 shows a velocity structure taken from Naini and Leyden (1973). Their interval velocity solutions

were plotted at the midpoint of the corresponding layers and velocity gradients were assumed in such a way as to minimize discontinuities. The most obvious feature of the velocity-depth model is a thin, almost isovelocity layer which is of prominently higher velocity than the surrounding structure. To investigate the refracted rays in such a structure, a computer ray tracing was performed (Figure 9).

Examination of Figure 9 shows that there are apparently no rays refracted in layer 4. The ray  $\theta_o = 26^\circ$  ( $\theta_o$  is the angle at which the ray leaves the shot point) does not turn over in the layer and the ray  $\theta_o = 27^\circ$  reflects from the upper interface. The rays which do refract in layer 4 are in the range  $\theta_o = 26.34^\circ$  to  $\theta_o = 26.77^\circ$ ; since they are from such a small range of angles, they carry very little energy. Returns of such low amplitude probably would not be seen in the seismic signal.

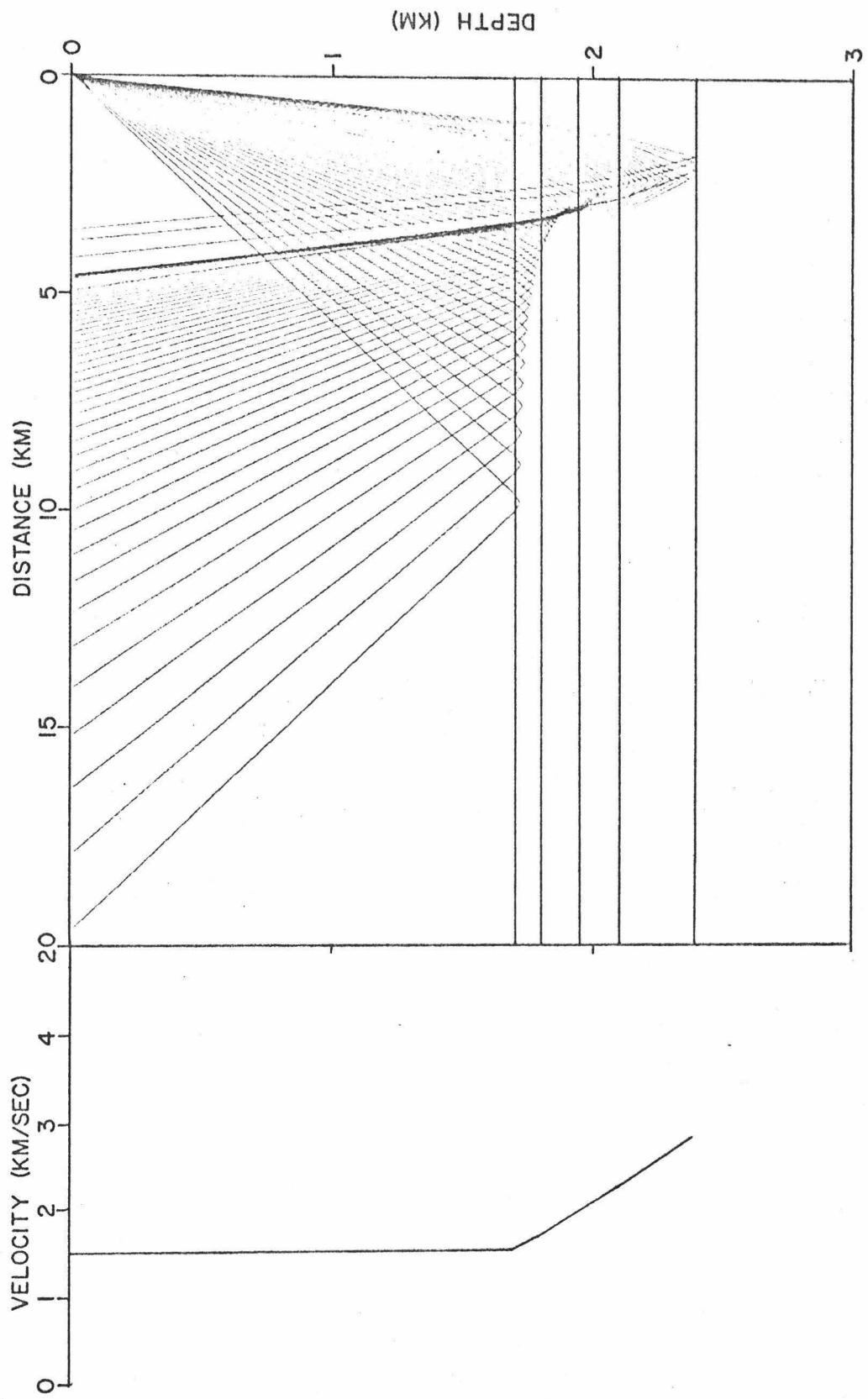
To investigate the consequences of missing a layer, the travel time curves for the Naini and Leyden structure were analyzed with the method of this paper. The travel time curve from layer 4 (the anomalous layer) was ignored and a solution for the lowest layer was sought on the basis of the curve from layer 5. A typical result is shown as the dashed line in Figure 9. The gradient for this composite layer is some 40% too low and the velocity at its upper interface is somewhere between the velocities at the tops of the two actual layers. The thickness of the

composite layer, however, is only 1% off the combined thicknesses of layer 4 and layer 5. This indicates that total internal refractions probably will not resolve severe irregularities in the velocity-depth structure but that the solutions obtained will be a satisfactorily averaged approximation.

The other problem arising from the physical velocity structure is illustrated by Figure 10. The model is an interval velocity solution from Maynard (1973) with gradients assumed as before. What appears to be one large second layer is actually four layers with no primary discontinuities and very similar gradients ( $1.6-2.0 \text{ sec}^{-1}$ ).

Examination of the ray tracing shows that rays refracted in the deeper layers emerge at the surface over a very limited range. Rays refracted in layer 5 emerge between 4.4 and 4.9 km; from layer 4 between 4.9 and 5.6 km; from layer 3 between 5.6 and 8.2 km; and from layer 2, rays emerge from 8.2 km outward. It is probable that the travel time curves from layers 4 and 5 would not be observed in actual experiments due to their extremely short length. This result indicates that the  $R_s$  method probably will be limited to the interpretation of arrivals from the first few hundred meters of sediments. However, this restriction is not as severe as it sounds since in many areas the sediment cover is very thin.

Figure 10. Velocity structure and ray paths for model  
from Maynard (1973). Rays traced for  
 $\theta_o = 30^\circ$  to  $\theta_o = 85^\circ$ .



General problems

Problems of the general type arise from the deviation of real media from the simple geometric model upon which the theory is based. This category includes such phenomena as dispersion, anisotropy, and attenuation, and it ultimately limits the application of all seismic methods. The two problems most widely discussed in relation to wide-angle reflection work are topography and water column structure.

Local topography is the most serious. Its deleterious effects have been discussed by nearly every author on the subject (e.g. Dix, 1955; Le Pichon et al., 1968; Maynard, 1973). The requirement of reasonably flat, non-sloping layers already limits the use of the ASPER method over much of the ocean floor.

The fine velocity structure of the water column becomes a problem in applying the method to thin layers. Bryan (1974) points out that the erroneous assumption of constant velocity in the water introduces errors directly to the reduced travel time data for the layers below. When the layer thicknesses become less than 8-10% that of the water column, these errors produce unacceptable interval velocity solutions.

To test the effect of a layered water column, refraction travel time curves were calculated for two cases of

Maynard's velocity-depth model shown in Figure 8. One case assumed a layered water column with velocity gradients (Fry and Raitt, 1961, p. 592) and the other an isovelocity water column with an equivalent average velocity (1.485 km/s). In both cases the column was 1.70 km thick.

As expected (Le Pichon et al., 1968), the layered water column made little difference except at wide angles of incidence. At ranges out to 8 km, travel times between the two cases differed by less than 3 msec; at a range of 17 km the difference had increased to about 10 msec. Referring to the ray tracing of this particular structure (Figure 8) it is evident that most of the error occurs in ray paths refracted in the second layer. Since the one-way travel time in the second layer is only about .06 sec (approximately 5% of the water column), it is evident that this discrepancy is significant. Some options presented by this problem are, a) accept the 8-10% minimum criterion, b) assume a water column structure and correct travel times accordingly, or c) use an ocean bottom receiver to cut the effect by half.

#### Experimental problems

The final category of problems arises from the nature of the ASPER experimental system (Maynard et al., 1974). There are several drawbacks in the system at present. For

instance, the data collected is often noisy. Also, since the facsimile record is made on wet paper, it is subject to some amount of distortion with time. By far the major problem, however, is the pulse length of the sound source. The pulse length of a typical air gun can be as much as .10 to .25 sec. Maynard et al., (1974) show that  $R_s$  arrivals approach reflection arrivals asymptotically as range increases; since the difference in arrival time is often on the order of hundredths of a second, it is apparent that refracted arrivals will frequently be lost in the pulse train of the reflected return. This is no doubt the major reason that no  $R_s$  rays were identified on the records reviewed.

There are some indications, on the other hand, that the refraction ray path method can be successfully applied. First,  $R_s$  returns have been used to estimate velocity gradients in previous experiments using explosive sound sources (Hill, 1952; Katz and Ewing, 1956; Ewing and Nafe, 1963). In these experiments, the seismic signal was recorded as a waveform on a chart recorder; this mode of recording facilitates identification of the  $R_s$  returns and allows accurate timing of its arrival. The major drawbacks of this type of experiment are the relatively low data density and the inconvenience of working with explosives and large numbers of chart records.

A second encouraging point is that the  $R_s$  method shows good statistical accuracy in estimating the gradient for the upper layers of geologically reasonable models. Travel time curves were generated for Maynard's velocity structure (Figure 10) and analyzed with the program described in Section III. Table 2 shows estimates of the velocity gradient of each layer below the water column for various magnitudes of timing error. Considering only layers 2 and 3, notice that the worst estimate is about 27% too low. Note also that for  $\sigma = .002$  sec (a reasonable estimate of the present accuracy of the system) the errors are not far beyond 10%. It appears that the  $R_s$  method will be quite accurate in solutions for the upper sediment layers but it should be noted that these results were obtained without any physical complications to the simple, plane-bounded model.

At this point, the evidence indicates that the method probably is not, at present, generally feasible: no applicable data was found, and model studies show there to be several restrictions to the method's application. The lack of data most likely can be attributed, however, to the experimental problems discussed before. The success of previous investigators in using  $R_s$  data is probably due to their mode of recording. It would be advantageous if the accuracy of the chart recorder could be coupled with the efficiency and high data density of the ASPER system.

Table 2. Estimates of the velocity gradient in layers of model taken from Maynard (1973) (ASPER D-12).

<u>Layer</u>	<u>True <math>\gamma</math></u>	<u>Estimated <math>\gamma</math></u>			
		<u><math>\sigma = .001</math></u>	<u><math>\sigma = .002</math></u>	<u><math>\sigma = .003</math></u>	<u><math>\sigma = .004</math></u>
2	1.60	1.64 (2.4%)	1.42 (-10.9%)	1.16 (-27.6%)	1.62 (-1.1%)
3	1.80	1.89 (5.2%)	1.67 (-7.2%)	2.10 (16.5)	1.77 (-1.8%)
4	1.87	.58 (-69.3%)	1.64 (-12.4%)	1.68 (-10.1%)	0 (-100%)
5	2.00	1.45 (-27.5%)	1.81 (-9.5%)	1.73 (-13.4%)	1.36 (-32.0%)

A large step toward this goal would be accomplished by digitally recording the signal. With the signal in digital format, several different types of processing can be employed to substantially improve the quality of the record. First, the signal can be frequency filtered selectively to enhance returns from a specific depth. By doing this, an optimum tradeoff between resolution and penetration can be achieved. Second, timing accuracy can be increased because the signal can be displayed as a waveform. In the waveform representation the onset of an arrival can be identified more exactly than in the equivalent facsimile record.

The most important improvement will come from predictive deconvolution to remove the reverberation effects from a seismic source. Most of the difficulty in picking travel times from ASPER records is due to interference among overlapping wave trains. The problem is particularly acute at large ranges where closely spaced arrivals are obscured by the strong first bottom return. Deconvolution would clarify the record by shortening the wave train of each return. On a deconvolved record, it would be, for instance, much easier to differentiate reflections, total internal refractions and head wave refractions. In many cases, arrivals from these ray paths are very close in time. Maynard, et al., (1974) discuss the consequences of misidentifying the ray path.

On the assumption that the experimental procedure can be improved, it is important to note that the  $R_s$  method has a major potential advantage. That is, it provides a consolidated approach to the estimation of velocity gradients from ASPER data. Most previous investigators (e.g. Knox, 1965; Hamilton et al., 1974) have estimated gradients by performing a large number of reflection experiments and plotting the interval velocity solutions as a function of depth. The plotted points are then fit with a polynomial by least squares, and from this the gradient is calculated.

Using that approach, a large number of determinations must be made to assure a statistically accurate result. Thus the velocity gradient can only be specified on a regional basis. The analysis of  $R_s$  rays, on the other hand, can determine gradients from individual ASPER records with good statistical accuracy. The velocity gradient, at least in the upper sediments, then can be specified locally.

The new method is also potentially useful in resolving the velocity in the sediments at the interface with the water column. Different investigations of this parameter give markedly different results. For instance, working in the Bay of Bengal, Naini and Leyden (1973) project the sediment surface velocity to be 1.83 km/sec. Hamilton et al. (1974), working in the same area, assume the velocity at 1.48 km/sec. Since our theoretical model is

parameterized in terms of the velocity at the top of the layer,  $b$ , an analysis of  $R_s$  rays should provide information to help resolve this discrepancy.

### Conclusions

In the summary, then, it has been shown that the parametric travel time equations are a convenient representation of multi-layer travel time data because they provide a precise method for point-by-point reduction to the single layer case. The single layer case is then readily solved using a non-linear model and Davidon's method. Whereas for reflection data the procedure is not effective for estimating gradients, acceptable results can be achieved using  $R_s$  travel times.

Whether or not the procedure can be successfully applied to real data is still not known. That the procedure is potentially a very accurate way of studying the upper sediments indicates that it should be tested. Before this test is possible, however, the ASPER system must be improved.

As a guide to conducting an evaluation of the method, the following suggestions are offered. First, and most obvious, the data should be taken over a sediment column which is as close an approximation to the model as possible. In this regard, the Ontong-Java Plateau appears a good choice. As noted before, the layers are flat and almost

non-sloping and most likely have strong velocity gradients. In addition, the water column is relatively shallow (roughly 2 km) and the area has been well drilled (DSDP sites 64, 288, and 289).

Second, as discussed before, the signal should be recorded digitally over a wide frequency range. The wide-band recording will allow various filtering strategies to be employed after the experiment. Also, even with little or no processing, examination of the signal as a waveform might help identify  $R_s$  returns. Finally, the reflection/refraction experiments should be additionally conducted at very high frequency (3.5 kHz). While sacrificing penetration, the high frequency sound source yields both high resolution and an extremely short pulse train (10 msec).

Even with the successful identification of  $R_s$  returns, it is apparent that the method is not comprehensive; there are restrictions on the application of the method over the whole sediment column. However, used in conjunction with reflection and head wave refraction data,  $R_s$  data analysis can provide a check for internal consistency and a more complete use of all the information available on an ASPER record.

APPENDIX A: Parametric Travel Time Equations  
Elliptically Anisotropic Case

The parametric equations for reflections in an anisotropic layer are derived in the same way as the equations of Section II. Again assume a flat, homogeneous layer as in Figure 2. In this case, however, the seismic velocity varies elliptically with angle;

$$v(\theta) = \left( \frac{\cos^2 \theta}{v_V^2} + \frac{\sin^2 \theta}{v_H^2} \right)^{-1/2} \quad (A1)$$

where  $v_V$  = velocity in the direction  $\theta = 0$

$v_H$  = velocity in the direction  $\theta = \pi/2$

Application of Fermat's principle and the calculus of variations leads to the parametric equations for reflections from the lower interface of the layer:

$$\begin{aligned} x &= 2h v_H^2 p / v_V (1 - p^2 v_H^2)^{1/2} \\ t &= 2h / v_V (1 - p^2 v_H^2)^{1/2} \end{aligned} \quad (A2)$$

where  $h$  = layer thickness and  $p$  is the ray parameter and again is constant over a given ray path.

Note that in the anisotropic case,

$$p = \frac{\sin \theta v(\theta)}{v_H^2} = \frac{\sin \theta}{v_H^2 \left( \frac{\cos^2 \theta}{v_V^2} + \frac{\sin^2 \theta}{v_H^2} \right)^{1/2}}$$

If the parameter  $p$  is eliminated from equations (A2), a single equation defines the travel time curve:

$$t^2 = \frac{x^2}{v_H^2} + \frac{4h^2}{v_V^2} \quad (A3)$$

Equation A3 describes a straight line in  $t^2-x^2$  which is indistinguishable from the travel time curve of an isotropic, isovelocity layer. A straight line has only two degrees of freedom but the anisotropic case requires three parameters. Therefore, the problem is under-determined.

An erroneous assumption of isotropy ( $v_V = v_H$ ) thus introduces error in the determination of thickness. Therefore, if one assumes elliptical anisotropy, the 5-10% anisotropies observed by Kroenke (personal communication, 1974) could mean 5-10% errors in many thickness determinations. Vossler (Vossler and Castain, 1972; personal communication, 1975), on the other hand, argues that the model of elliptical anisotropy is not physically realizable and proposes instead a model of transverse anisotropy. His simulations, however, show that P waves are very insensitive to the degree of anisotropy and suggest that shear wave data are required to solve the problem.

## APPENDIX B: Interval Velocities--Parametric Approach

Slotnick (1959, p. 180, equation (5)) gives the parametric travel time equations for reflections in a flat, homogeneous isotropic layer as

$$\begin{aligned} x &= 2h v p / (1 - p^2 v^2)^{1/2} \\ t &= 2h / v (1 - p^2 v^2)^{1/2} \end{aligned} \quad (B1)$$

where  $v$  = velocity of layer

$h$  = thickness

Consider again  $m$  observations of a travel time curve,  $(x_i, t_i; i = 1, \dots, m)$ . Assume that the associated  $p_i$  have been calculated by fitting a least squares curve as described in Section III. For some arbitrary  $x_i, t_i,$  and  $p_i,$  simple algebra shows that, from equation (B1),

$$v = \left( \frac{x_i}{t_i p_i} \right)^{1/2} \quad (B2)$$

Thus, determinations of the interval velocity can be made at  $m$  points along the travel time curve. The technique has several advantages, among them: 1) random error can be minimized by averaging the  $m$  estimates and 2) trends in the estimates as a function of range can be used to judge the validity of the isovelocity assumption. Note that the method is valid in the multi-layer case when the  $(x_i, t_i)$  are reduced time and distance.

## REFERENCES

- Beale, E. M. L., 1960, Confidence regions in non-linear estimation, *J. Roy. Statis. Soc.*, B-22, p. 41-76.
- Bryan, G. M., 1974, Sonobuoy measurements in thin layers, Physics of Sound in Marine Sediments, Loyd Hampton, ed. Plenum Press, N. Y., p. 119-129.
- Clay, C. S. and P. A. Rona, 1965, Studies of seismic reflections from thin layers on the ocean bottom in the Western North Atlantic, *J. Geophys. Res.*, v. 70, p. 855-869.
- Davidon, W. C., 1959, Variable metric method for minimization, (Brit.) Atomic Energy Comm. Res. and Devel. Rept. AL5990 (Rev).
- Dix, C. H., 1955, Seismic velocities from surface measurements, *Geophysics*, v. 20, p. 63-86.
- Ewing, J. I. and J. E. Nafe, 1963, The unconsolidated sediments in The Sea, v. 3, M. N. Hill, ed., J. Wiley and Sons, N. Y., p. 73-84.
- Fletcher, R. and M. J. D. Powell, 1963, A rapidly convergent descent method for minimization, *Computer J.*, v. 6, p. 163-168.
- Fry, J. C., and R. W. Raitt, 1961, Sound velocities at the surface of deep sea sediments, *J. Geophys. Res.*, v. 66, p. 589-597.
- Green, C. H., 1938, Velocity determinations by means of reflection profiles, *Geophysics*, v. 3, p. 295-305.
- Hamilton, E. L., 1965, Sound speed and related physical properties of sediments from experimental Mohole (Guadalupe Site), *Geophysics*, v. 30, p. 257-261.
- Hamilton, E. L., 1970, Sound velocity and related properties of marine sediments, *No. Pacific, J. Geophys. Res.*, v. 75, p. 4423-4446.
- Hamilton, E. L., D. G. Moore, E. C. Buffington, and P. L. Sherrer, 1974, Sediment velocities from sonobuoys: Bay of Bengal, Bering Sea, Japan Sea, and North Pacific, *J. Geophys. Res.*, v. 79, p. 2653-2668.

- Hill, M. N., 1952, Seismic refraction shooting in an area of the eastern Atlantic, Phil. Trans. R. Soc. London, A244, p. 561-596.
- Houtz, R. E., J. Ewing, and X. Le Pichon, 1968, Velocity of deep-sea sediments from sonobuoy data, J. Geophys. Res., v. 73, p. 2615-2641.
- Katz, S. and M. Ewing, 1956, Seismic refraction measurements in the Atlantic Ocean Part VII: Atlantic Ocean Basin, west of Bermuda, Bull. Geol. Soc. Amer., v. 67, p. 475-510.
- Knox, W. A., 1965, A deep-ocean sedimentary velocity function, J. Geophys. Res., v. 70, p. 1999-2001.
- Le Pichon, X., J. Ewing, and R. E. Houtz, 1968, Deep-sea velocity determination made while reflection profiling, J. Geophys. Res., v. 73, p. 2597-2614.
- Maynard, G. L., 1973, Seismic wide angle reflection and refraction investigation of the sediments on the Ontong Java Plateau, doctoral dissertation, Univ. of Hawaii.
- Maynard, G. L., G. H. Sutton, D. M. Hussong, and L. W. Kroenke, 1974, The seismic wide angle reflection method in the study of ocean sediment velocity structure, Physics of Sound in Marine Sediments, Loyd Hampton, ed., Plenum Press, N. Y.
- Naini, B. R. and R. Leyden, 1973, Ganges Core: A wide angle seismic reflection and refraction study, J. Geophys. Res., v. 78, p. 8711-8720.
- Slotnick, M. M., 1959, Lessons in Seismic Computing, Soc. of Expl. Geophysicists, Tulsa.
- Vossler, D. A. and J. K. Castain, 1972, Anisotropic media and the determination of subsurface velocity by use of seismic reflection data (abstract), SEG Program with Abstracts, 1972.